Proton motive force dissipation drives flavodiiron proteins to the thylakoid membrane for ferredoxin-powered O_2 photoreduction

Lauri Nikkanen[1], Serhii Vakal[2], Anita Santana-Sánchez[1], Michal Hubacek[1], Yingying Wang[3], Marko Böhm[4], Kirstin Gutekunst[3,4], Tiina A. Salminen[2], and Yagut Allahverdiyeva[1*]

[1] Molecular Plant Biology, Department of Life Technologies, University of Turku, FI-20014 Turku, Finland

[2]Structural Bioinformatics Laboratory and InFLAMES Research Flagship Center, Faculty of Science and Engineering, Åbo Akademi University, FI-20520, Turku, Finland

[3]Plant Cell Physiology and Biotechnology, Botanical Institute, University of Kiel, D-24118 Kiel, Germany

[4]Molecular Plant Physiology, University of Kassel, D-34132 Kassel, Germany

* corresponding author

Absract

Flavodiiron proteins (FDPs) catalyse light-dependent reduction of oxygen to water in photosynthetic organisms such as cyanobacteria, creating a protective electron sink that alleviates electron pressure on the photosynthetic apparatus. However, the electron donor to FDPs and the molecular mechanism regulating FDP activity have remained elusive. To address these questions, we employed spectroscopic and gas flux analysis of photosynthetic electron transport, bimolecular fluorescence complementation assays for *in vivo* protein-protein interactions in the model cyanobacterium *Synechocystis* sp. PCC 6803, as well as *in silico* surface charge modelling. We confirmed Ferredoxin-1 as the main electron donor to FDP heterooligomers and revealed that association of FDP heterooligomers with thylakoid membranes is promoted by dissipation of trans-thylakoid proton motive force. We propose a self-feedback mechanism to dynamically control FDP activity. Our findings elucidate the regulatory mechanisms of photosynthesis and have implications for rationally directing electron flux toward desired reactions in photosynthesis-based biotechnological applications.

Introduction

In oxygenic photosynthetic organisms apart from angiosperms and red and brown algae, class C flavodiiron proteins (FDPs) catalyse light-dependent reduction of O_2 to H_2O. This process, referred to as the Mehler-like reaction, creates a strong electron sink on the acceptor side of Photosystem I (PSI) and alleviates excessive reduction of the photosynthetic electron transport chain (PETC), protecting the photosynthetic apparatus from photodamage. It has been proposed that, unlike in the Mehler reaction, no harmful reactive oxygen species (ROS) are produced[1,2]. Indeed, the Mehler-like reaction is essential for the growth of cyanobacteria[3], unicellular algae[4], and moss[5] in conditions mimicking natural fluctuations of light intensity. FDPs are also common in non-photosynthetic bacteria, archaea and eukaryotes, and are classified into classes A-H depending on their domain composition[6]. All FDPs share a core modular domain structure containing a metallo β-lactamase-like domain with a non-heme diiron catalytic site and a flavodoxin-like domain with a flavin mononucleotide (FMN) binding site[6]. Some FDPs, including in photosynthetic algae, catalyse the reduction of nitric oxide (NO) to nitrous oxide (N_2O), while yet others can reduce both NO and O_2[6–8].

The model cyanobacterium *Synechocystis* sp. PCC 6803 (hereafter *Synechocystis*) has four FDP isoforms (Flv1-Flv4)[9] that likely form various homo- and heterooligomeric conformations. The Mehler-like reaction is catalysed by heterooligomers consisting of Flv1 and Flv3 or Flv2 and Flv4[3,9–11]. Although it has been established that FDPs function as a release valve for excessive electrons on the acceptor side of PSI[3,9,10], and that the Mehler-like reaction is dependent on the presence of all FDPs under air-level CO_2[10,11], the identity of the electron donor(s) to FDPs has remained uncertain. Based on *in vitro* experiments with recombinant proteins, it was suggested that NAD(P)H would function as the main electron donor to Flv1, Flv3, and Flv4[2,12,13]. However, in those experiments FDPs were present as homooligomers, whose physiological function remains unknown but has been shown to be distinct from O_2 photoreduction[11]. Given the distinct kinetic profiles of O_2 photoreduction catalysed by Flv1/3 and Flv2/4 heterooligomers under air-level CO_2 concentrations[10], the *in vivo* electron donor to different heterooligomers, and to the unknown reactions catalysed by FDP homooligomers, could differ. While Flv3 and Flv2 homooligomers and Flv2/4 heterooligomers have been biochemically detected in *Synechocystis*[11,14], Flv1/3 heterooligomers have not been directly observed, and the abilities of FDPs to interact with each other and to form different oligomeric forms have not been fully explored.

Alternative electron donors such as ferredoxin (Fed) or (ferredoxin:$NADP^+$ oxidoreductase (FNR) were not tested in the aforementioned *in vitro* studies[2,12]. However, recent *in vivo* measurements of light-induced NAD(P)H and Fed redox changes in wild-type (WT) *Synechocystis* and Flv1/3-deficient mutant cells strongly support Fed as the main electron donor at least to Flv1/3 heterooligomers[15,16]. *Synechocystis* has eleven Fed isoforms (Fed1-Fed11)[17] but only little is known about their specific functions or the extent of redundancy between them. Fed1-6 are "plant-type" ferredoxins harbouring a [2Fe-2S] cluster, while Fed7, 8, and 9 are bacterial types with [4Fe-4S], [3Fe-4S] [4Fe-4S], and [4Fe-4S] [4Fe-4S] iron-sulphur cluster compositions, respectively[17–19]. Previously, Fed9 has indeed been shown to interact with Flv3 in a bacterial two-hybrid system[18], and Flv1 and Flv3 with Fed1 in a Fed-affinity chromatographic assay[20]. Moreover, the Δ*Fed7*

mutant has a lowered expression level of the *flv2-4* operon and decreased photosynthetic efficiency under high irradiance and air-level [CO_2][21]. Evidence of *in vivo* interaction is however lacking.

To resolve these ambiguities, we developed a bimolecular fluorescence complementation (BiFC) platform to study protein–protein interactions in living cyanobacterial cells, which we then utilised to examine the capability of FDPs to interact *in vivo* with putative electron donors as well as with each other. BiFC takes advantage of reassembly of a fluorescent protein (FP) upon proximity of two co-expressed fusion proteins consisting of a protein of interest and an N- or C-terminal fragment of an FP[22–24]. The FP is then excited at the appropriate wavelength, and the resulting fluorescence emission from interactions is typically detected by a confocal microscope. A substantial benefit of BiFC tests in comparison to *in vitro* methods such as co-immunoprecipitation, or methods based on exogenous expression such as two-hybrid systems, is that it can also provide information on the *in vivo* subcellular localisation of the detected protein–protein interactions. Although BiFC has been extensively used to study interactions in plant cells and chloroplasts[24–27], it has not, to our knowledge, been previously utilised in cyanobacteria. BiFC has however been successfully employed in other bacterial model organisms such as *E. coli, B. subtilis,* and *A. tumefaciens*[22] and background fluorescence caused by cyanobacterial phycobilisomes or chlorophyll (Chl) does not interfere with the use of fluorophores such as GFP, YFP or CFP[28].

To reveal if any of the low abundance Fed isoforms in *Synechocystis* (Fed2-Fed11), NADPH, or FNR are required for the Mehler-like reaction, we performed biophysical characterisation of deletion strains deficient in low abundance Feds and FNR. We then used the BiFC platform to elucidate the protein–protein interactions and subcellular localisations of different FDP isoforms. Our combined approach of biophysical characterisation and BiFC assays allowed us to demonstrate that Fed1, not NADPH or FNR, is the main electron donor to the light-induced Mehler-like reaction catalysed by Flv1/3 and Flv2/4 heterooligomers. Moreover, the subcellular localisation of the interactions between FDPs and between FDPs and Fed1 provided evidence that the magnitude of the trans-thylakoid proton gradient controls reversible association of different Flv1/3 and Flv2/4 heterooligomers with the thylakoid membrane. Moreover, *in silico* modelling of FDP heterooligomer surface charges supported pH-dependent electrostatic binding to thylakoid membranes. Based on these findings and our previous biophysical studies we propose a self-feedback mechanism for precise post-translational regulation of Fed1-driven O_2 photoreduction activity of FDP heterooligomers.

RESULTS

Flv3 interacts with FNR on thylakoids but FNR and NADPH are not main reductants of Flv1/3 heterooligomers

First, we investigated the possibility of FDPs interacting directly with, and/or being reduced by FNR. There are two FNR isoforms in *Synechocystis*, FNR_L and FNR_S. The larger FNR_L form functions as the main photosynthetic carrier of electrons from Fed to $NADP^+$, while the smaller FNR_S form, deriving from later initiation of transcription of the *PetH* gene, is upregulated under nutrient starvation or in heterotrophic conditions[29]. FNR_S was recently suggested to catalyse

NADPH oxidation during cyclic electron transport upon dark-light transitions, providing reduced Fed for NDH-1[30]. To investigate if either FNR_L or FNR_S is involved in powering the Mehler-like reaction, we monitored real-time NADPH redox changes and light-induced O_2 exchange in knockout mutant strains ΔFNR_L and ΔFNR_S (also called FSI and MI6, respectively)[29]. Measurement of NADPH fluorescence revealed that light-dependent $NADP^+$ reduction was impaired in ΔFNR_L (Fig. 1a), in agreement with the previous observation that NADPH/$NADP^+$ ratio is lowered in the mutant[31]. No difference to WT was detected in ΔFNR_S.

In WT cells, a strong but transient peak of O_2 photoreduction during the first minute after the onset of illumination is catalysed mainly by Flv1/3 heterooligomers with some contribution from Flv2/4, while the steadier O_2 photoreduction thereafter is mostly dependent on Flv2/4[10] (Fig. 1b). If NADPH was the electron donor to FDP heterooligomers, the shortage of light-induced NADPH production in ΔFNR_L cells should result in inhibition of the Mehler-like reaction. However, no significant impairment of maximal O_2 photoreduction rate was detected in either ΔFNR_L or ΔFNR_S, when O_2 fluxes were monitored by time-resolved membrane-inlet mass spectrometry (MIMS), with O_2 uptake distinguished from O_2 evolution by enriching the medium with $^{18}O_2$ (Fig. 1c). A small, statistically non-significant decrease in maximum O_2 photoreduction was, however, observed in ΔFNR_L. This was likely caused by a diminished amount of Flv2 protein in the mutant (Fig. 1d). An elevated level of dark respiration was also detected in ΔFNR_L cells (Supplemental Fig. 1b), possibly due to the increased amount of FNR_S in ΔFNR_L (Fig. 1d)[29]. Taken together, these results indicate that neither FNR nor NADPH is a major electron donor to the Mehler-like reaction catalysed by Flv1/3 heterooligomers *in vivo*.

We also investigated potential protein–protein interactions between FNR_L and FDPs using the BiFC system. When Flv3 fused to an N-terminal Venus fragment (Flv3:VN) was co-expressed in WT *Synechocystis* cells with FNR_L fused to a C-terminal Venus fragment (FNR_L:VC), strong fluorescence emission at 519–570 nm was detected upon excitation at 488 nm, indicating successful reassembly of the Venus fragments and interaction between Flv3 and FNR_L (Fig. 1e). In order to assess the subcellular localisation of the interaction, we compared the average intensity of Chl *a* fluorescence, indicative of the location of the thylakoid membranes, with the fluorescence from re-assembled Venus proteins, over cross-sections of individual cells. As thylakoid membranes are mostly located along the edges of the cell in *Synechocystis*, the Chl regression line forms an M-shape over cell cross-sections. We also plotted the co-localised Chl and Venus fluorescence intensities against each other in a cytofluorograph and calculated the Pearson correlation coefficient (PCC) of Chl and Venus fluorescence co-localisation. Venus fluorescence from FNR_L-Flv3 interactions along cell cross sections closely matched that of Chl, and showed an average PCC of 0.66 ± 0.17. These analyses indicated that the FNR_L-Flv3 interactions localised consistently to the thylakoid membrane (Fig. 1e).

No interaction was detected between Flv1:VN and FNR_L:VC (Fig. 1f), or between Flv2:VC and FNR_L:VN or FNR_S:VN (Supplemental Fig. 2). All FDP:FNR BiFC strains showed strong expression of both fusion proteins (Supplementary Fig. 3).

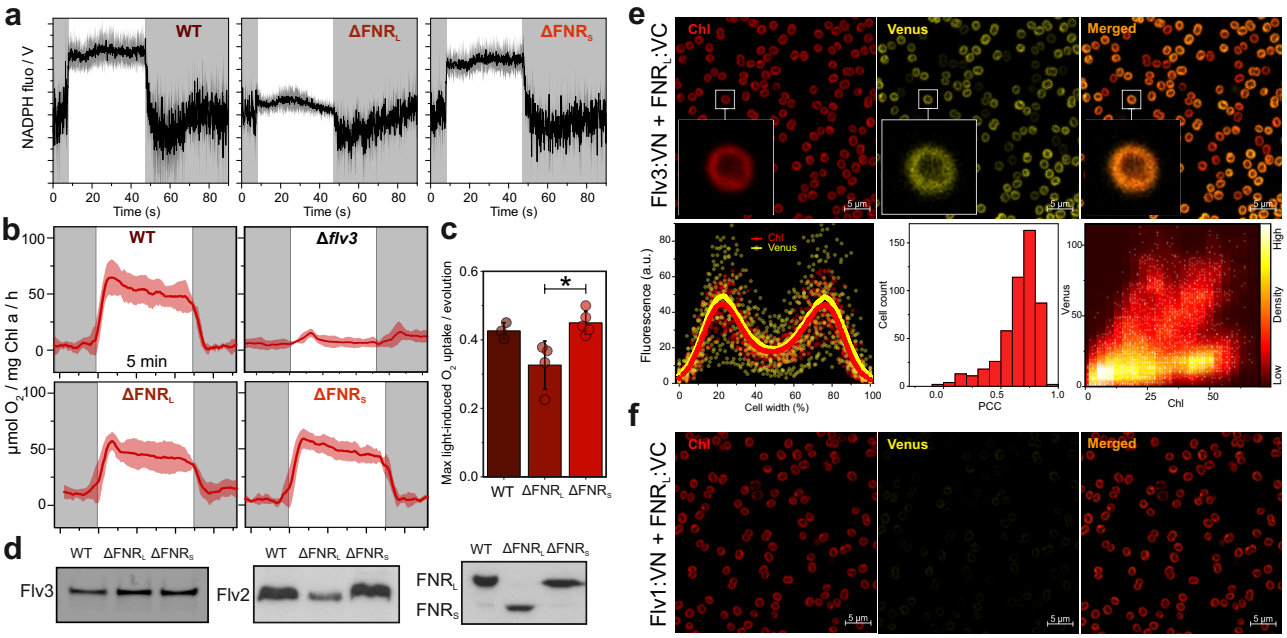

Fig. 1. Photosynthetic characterisation of FNR mutants and protein-protein interaction tests between FNR_L and FDPs.

(a) Light-induced NADPH fluorescence changes in WT, ΔFNR_L (no FNR_L, increased amount of FNR_S), and ΔFNR_S (no FNR_S, FNR_L present) cells during 40 s illumination at 500 µmol photons m^{-2} s^{-1} and subsequent darkness. Averaged traces from three biological replicates +/- standard deviation (shadowed area) are shown. Dark-adapted NADPH fluorescence levels were set to 0. **(b)** O_2 uptake kinetics measured by MIMS in WT, ΔFlv3, ΔFNR_L, and ΔFNR_S cells during 5 min illumination at 500 µmol photons m^{-2} s^{-1} and subsequent darkness. $^{18}O_2$ was added prior to the measurement in equal concentration to $^{16}O_2$ in order to distinguish O_2 uptake from O_2 evolution. Averaged traces from 3 (WT), 4 (ΔFNR_L), and 5 (ΔFNR_S) biological replicates +/- standard deviation (shadowed area) are shown. **(c)** The average magnitudes of the maximum O_2 photoreduction peaks normalised to the maximum O_2 evolution rate. Values are averages from 3 (WT), 4 (ΔFNR_L), and 5 (ΔFNR_S) biological replicates +/- standard deviation with individual data points shown as circles. * Denotes statistically significant difference according to Student's T-test ($P<0.05$). **(d)** Immunodetection of Flv3, Flv2, and FNR protein content in WT, ΔFNR_L, and ΔFNR_S cells using specific antibodies. **(e–f)** BiFC tests between Flv3 and FNR_L (e) and Flv1 and FNR_L (f). Representative confocal micrographs from three independent experiments are presented, showing chlorophyll a (Chl) autofluorescence emanating from the thylakoid membranes in the left panel, fluorescence from re-assembled Venus I152L fluorescent proteins in the middle, and overlaid Chl and Venus fluorescence on the right panel. The inlets show zoomed-in views of a single cell. For quantification of the subcellular localisations of the interacting fusion protein pairs, the co-localisation of Chl (red) and Venus (yellow) fluorescence is also presented with fluorescence intensities over 5-pixel-wide cross-sections of 30-40 cells (with width normalised to 100%) shown as a scatterplot. Brighter red and yellow lines show moving regression curves produced by locally weighted scatterplot smoothing (LOWESS). The histogram shows the distribution of the Pearson Correlation Coefficient (PCC) for Chl and Venus fluorescence co-localisation in all cells from three micrographs from individual replicates. A PCC of 1 indicates perfect co-localisation and a PCC of 0 no co-localisation. The cytofluorogram shows co-localised Chl and Venus fluorescence intensities as a scatter plot.

Deficiency of Fed2–11 does not impair the Mehler-like reaction

Having excluded FNR and NADPH as main electron donors to FDP heterooligomers, we proceeded to investigate how the lack of single or multiple Fed isoforms affects the Mehler-like reaction. To this end, we monitored light-induced reduction of O_2 in *Synechocystis* mutant strains deficient in Fed3, Fed4, Fed6, Fed 7, 8, and 9, Fed9, Fed10, or Fed11. Fully segregated mutants of Fed1, Fed2 or Fed5 cannot be obtained[19], but partially segregated deletion strains of Fed2 and Fed5 were nonetheless examined. We quantified the activity of the Mehler-like reaction as a ratio between maximum O_2 photoreduction and maximum gross O_2 evolution. In none of the Fed2-11 mutants was major impairment of the Mehler-like reaction observed (Fig. 2, Supplementary Fig. 4b). Slight decrease in O_2 photoreduction was however observed in cells deficient in bacterial-type ferredoxins (ΔFed789), while photoreduction of O_2 was moderately increased in ΔFed4 (Fig. 2b).

Deficiency of Flv1/3 results in a distinct inability to re-oxidise Fed and P700 at the onset of strong illumination[15,16,32]. Our MIMS results revealed that a lack of Fed4 slightly increased, and a lack of Fed9, which also interacts with Flv3 in two-hybrid tests[18], slightly decreased the rate of O_2 photoreduction. This prompted us to use a Dual-KLAS-NIR spectrophotometer to monitor the redox changes of Fed, P700, and plastocyanin (PC) upon illumination in ΔFed4 and ΔFed9 cells. Both ΔFed4 and ΔFed9 cells showed WT-like redox kinetics of Fed, PC, and P700 (Fig. 2c, Supplementary Fig. 5). These results confirm that low-abundance ferredoxins are not needed as main electron donors for the Mehler-like reaction, or as final electron acceptors in the photosynthetic electron transport chain.

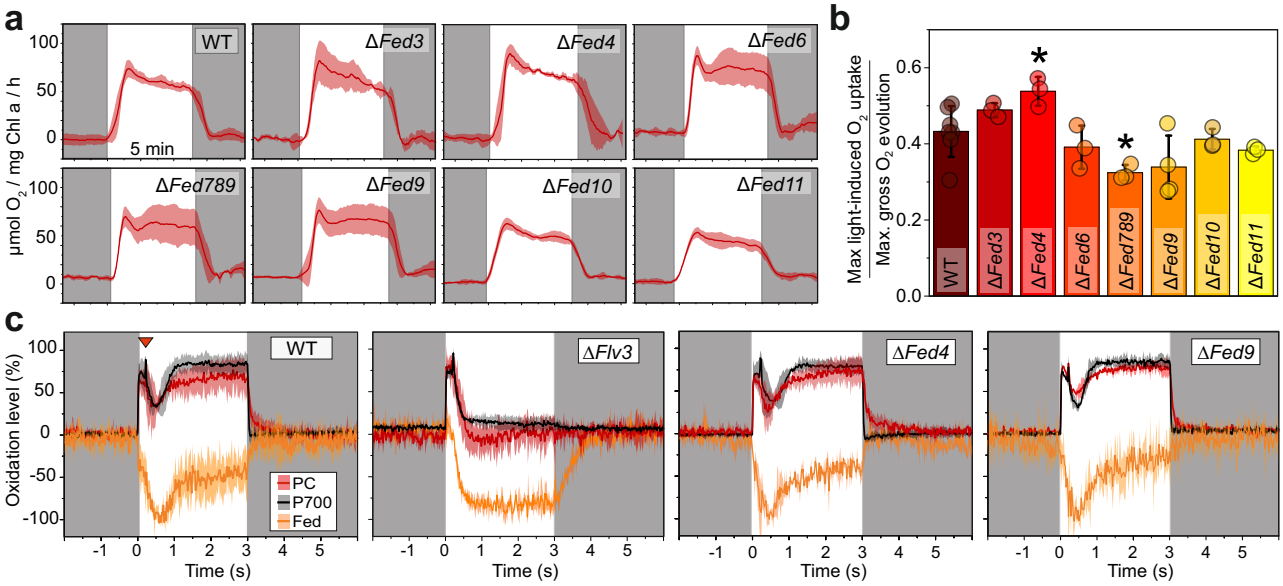

Fig. 2. Effect of low abundance Ferredoxins on the Mehler-like reaction. (a–b) O_2 photoreduction in cells deficient in low abundance Fed isoforms. O_2 gas exchange was monitored by MIMS before, during, and after 5 min of illumination with strong actinic light (500 μmol photons m^{-2} s^{-1}). (a) Averaged traces from 7 (WT), 3 (ΔFed3, ΔFed6, ΔFed789, ΔFed10, ΔFed11), or 4 (ΔFed4, ΔFed9) biological replicates with standard deviation. (b) Averages with standard deviation of peak O_2 photoreduction rate at c.a. 30 s of illumination normalised to the maximum gross rate of O_2 evolution. Data are averages from 3-7 biological replicates as in (a) and individual data points are shown as circles. * Signifies statistically significant difference to WT according to Student's T-tests ($P<0.05$). (c) Redox changes of PC, P700, and Fed in WT, ΔFed4, ΔFed9 and ΔFlv3 cells. Cells grown in air level CO_2 concentration for 4 days, harvested and

resuspended in fresh BG-11 pH 7.5 with Chl concentration adjusted to 15 µg/ml. PC, P700, and Fed redox changes were deconvoluted from near-infrared absorbance differences measured with a DUAL-KLAS-NIR spectrophotometer. A modified NIRMAX protocol was used, of which the 3 s illumination with 1750 µmol photons $m^{-2}s^{-1}$ actinic light is shown (see Supplementary Fig. 5 for the full experiment), including a multiple turnover pulse after 200 ms (indicated by the red triangle in the WT panel). The traces are normalised to the maximal oxidation values of PC and P700 and maximal reduction of Fed, as determined with the NIRMAX protocol. Averaged traces from 3 biological replicates are shown, with standard deviation as the shadowed area.

Fed1 interacts with FDPs

Fed1, the most abundant Fed isoform and the one mainly involved in photosynthetic electron transfer, is essential for survival of *Synechocystis* and a knockout mutant strain of it cannot be obtained[18,33,34]. We therefore proceeded to investigate potential interactions between Fed1 and FDPs using the BiFC system. When Fed1 fused to an C-terminal Venus fragment (Fed1:VC) was co-expressed in WT *Synechocystis* cells with Flv1 fused to an N-terminal Venus fragment (Flv3:VN), strong Venus fluorescence was detected, suggesting a protein-protein interaction between Fed1 and Flv1 (Fig. 3a). Fed1-Flv1 interactions co-localised with Chl autofluorescence, indicating that they occurred on the thylakoid membrane. In contrast, co-expression of Fed1:VN with Flv3:VC resulted in a Venus fluorescence signal that showed little co-localisation with Chl fluorescence, indicating a cytosolic localisation for Fed1-Flv3 interactions (Fig. 3b). Interestingly, a clear, largely cytosolic interaction was detected also between Fed1:VN and Flv2:VC (Fig. 3c), but Fed1:VC failed to interact with Flv4:VN (Fig. 3d), suggesting that Flv2/4 heterooligomers may also receive reducing power from Fed1,but that the interaction occurs strictly through Flv2.

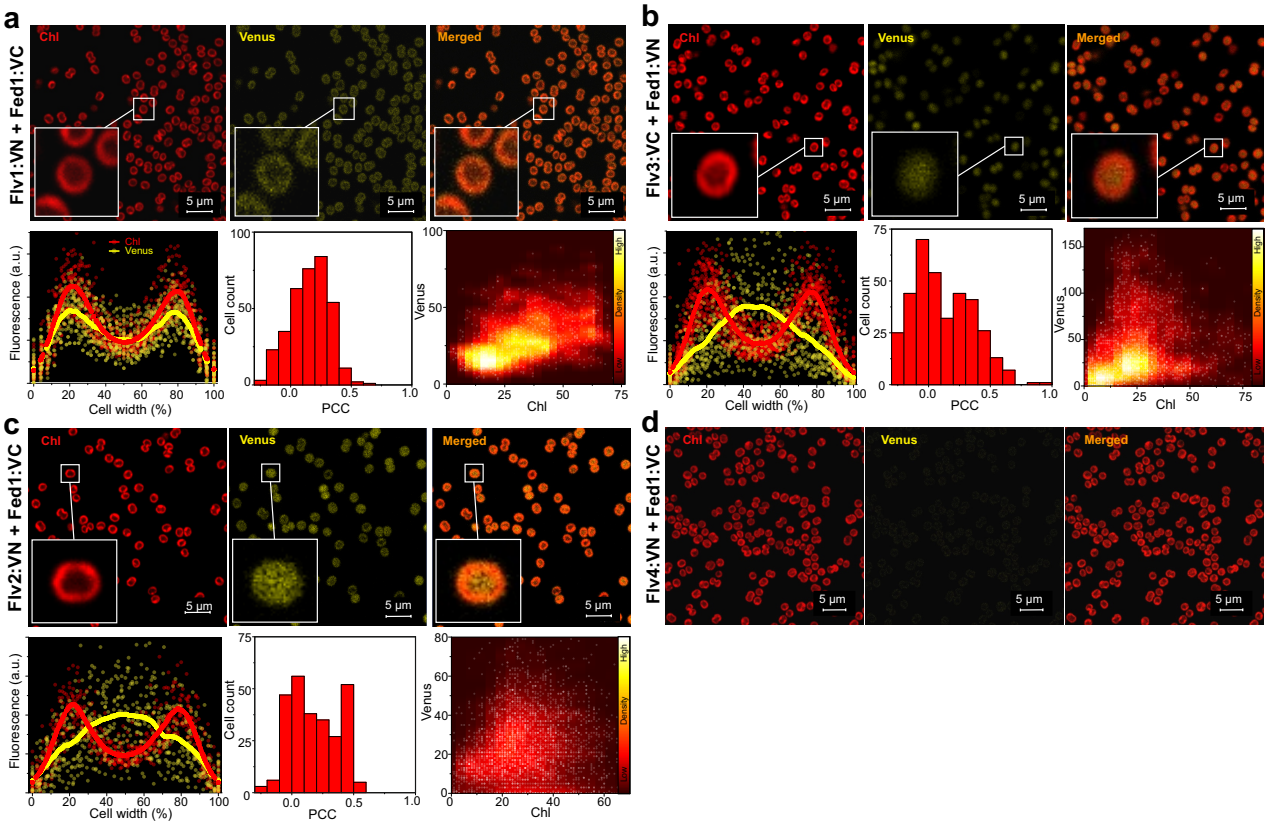

Fig. 3. Interactions between Fed1 and FDPs in BiFC tests. Representative confocal micrographs from 3 independent experiments are presented, showing chlorophyll a (Chl) autofluorescence emanating from the thylakoid membranes in the left panel, fluorescence from re-assembled Venus I152L fluorescent proteins in the middle, and overlaid Chl and Venus fluorescence on the right panel. (a) Flv1:VN + Fed1:VC, (b) Flv3:VC + Fed1:VN, (c) Flv2:VN + Fed1:VC, (d) Flv4:VN + Fed1:VC. For quantification of the subcellular localisations of the interacting fusion protein pairs, the co-localisation of Chl (red) and Venus (yellow) fluorescence is also presented with fluorescence intensities over cross-sections of 30-40 cells (with width normalised to 100%) shown as a scatterplot. Brighter red and yellow lines show moving regression curves produced by locally weighted scatterplot smoothing (LOWESS). The histograms show the distribution of the Pearson Correlation Coefficient (PCC) for Chl and Venus fluorescence co-localisation in all cells from three micrographs from individual replicates. A PCC of 1 indicates perfect co-localisation and a PCC of 0 no co-localisation. The cytofluorograms show co-localised Chl and Venus fluorescence intensities as a scatter plot.

Flv1/3 and Flv2/4 interactions exhibit *pmf* dependent association with the thylakoid membrane

Interactions between the FDP heterooligomer pairs, Flv1:VN and Flv3:VC (Fig. 4a), and Flv4:VN and Flv2:VC (Fig. 4b) were localised predominantly in the cytosol. In smaller subpopulations of cells, however, the interactions were localised at the thylakoids. This may indicate that the associations of Flv1/3 and Flv2/4 heterooligomers with the thylakoid membrane are dependent on the physiological state of the cell. We have suggested previously that such reversible membrane association, which would control the participation of FDP heterooligomers in O_2 photoreduction, may be mediated by changes in cytosolic or trans-thylakoid pH (the proton motive force, *pmf*)[35] or

by Mg^{2+} and Ca^{2+} cation concentration[14]. To investigate these hypotheses, we determined the localisation of interactions between FDP isoforms when suspended in a medium containing either a low or high Mg^{2+} and Ca^{2+} concentration, as well as in the presence of the proton gradient uncoupler carbonyl cyanide m-chlorophenylhydrazone (CCCP). Measurement of the 500-480 nm electrochromic shift (ECS) signal[36] confirmed that 30 µM CCCP is sufficient to diminish the *pmf* by elevating the proton conductivity of the thylakoid membrane while only moderately affecting photosynthetic proton flux (Supplementary Fig. 6). The initial generation of the *pmf* at dark-to-light transitions was decreased in low compared to high cation medium due to lower proton flux (vH+) (Supplementary Fig. 7).

Intriguingly, dissipation of the *pmf* due to addition of CCCP in the medium resulted in increased thylakoid localisation of both Flv1/3 (Fig. 4c) and Flv2/4 interactions (Fig. 4d). The average PCC of Flv1/3 and Flv2/4 interactions increased from 0.09±0.01(SEM) to 0.32±0.01 and from 0.06±0.01 to 0.33±0.01, respectively, upon addition of CCCP in the medium. No difference in the localisation of Flv1/3 or Flv2/4 interactions was detected between low or high cation concentration in the medium (Supplementary Fig. 8a–d). These results suggest that a low *pmf* induces association of FDP heterooligomers with the thylakoid membrane, likely elevating the rate of the Mehler–like reaction e.g. during dark-to-light transitions, while an increase in *pmf* and concomitant alkalisation of the cytosol would cause them to disassociate from the membrane. Indeed, addition of 15 µM CCCP, which results in dissipation of ~50% of the *pmf* (Supplementary Fig. 6), increased the peak O_2 uptake rate relative to maximum O_2 evolution from 49% to 64%, and 30 µM CCCP up to 87% (Supplementary Fig. 9a). Importantly, no O_2 photoreduction was detected in the presence of 30µM CCCP in the ΔFlv3 mutant (Supplementary Fig. 9b). A high O_2 photoreduction rate (up to 80-90% of gross O_2 evolution) is also maintained in the mutant strain lacking the NdhD1 and NdhD2 subunits of the NDH-1 complex (ΔD1D2)[15] or upon addition of 1mM potassium cyanide (KCN), an inhibitor of respiratory terminal oxidases[3]. Acridine yellow and -orange fluorescence measurements[37] showed that alkalisation of the cytosol is delayed both in the ΔD1D2 strain as well as in presence of 1mM KCN (Supplementary Fig. 10), suggesting that maintaining a more acidic cytosolic pH for longer allows FDP heterooligomers to remain at the thylakoid membrane and to sustain a high rate of O_2 photoreduction. Accordingly, no increase in O_2 photoreduction in the presence of KCN is detected in the ΔFlv1/Flv3 mutant[3].

Flv1 interacted with itself, and similarly to Flv1-Fed1 interactions, primarily on the thylakoids (Fig. 5a), suggesting either homooligomerisation or involvement in higher-order heterooligomers. Flv3 self-interactions showed more variation in their subcellular localisation, with two distinct populations of cells. Most cells exhibited relatively weak interaction signals localising on thylakoids while stronger signals localising in the cytosol were detected from a subpopulation of cells (Fig. 5b). Cation concentration had no clear effect on the subcellular localisation of Flv3 self-interactions, but the interaction signal was stronger in a high cation concentration than in low, while addition of CCCP decreased the amount of cytosolic Flv3 self-interactions (Supplementary Fig. 11).

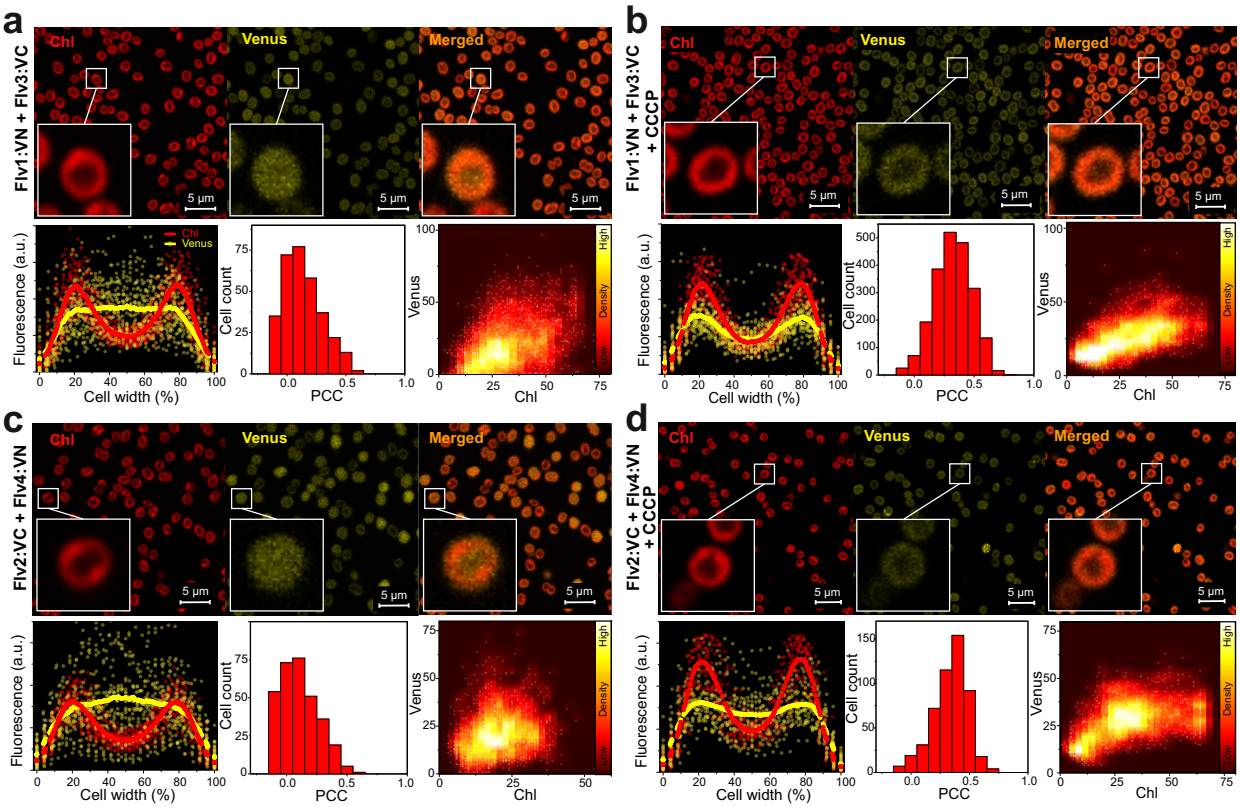

Fig. 4. Subcellular localisations of Flv1/3 and Flv2/4 interactions in BiFC tests. (a) BiFC tests between Flv1:VN and Flv3:VC. (b) BiFC tests between Flv1:VN and Flv3:VC with 30 µM CCCP added in the medium. (b) BiFC tests between Flv2:VC and Flv4:VN. (d) BiFC tests between Flv2:VC and Upper panels show representative confocal micrographs from the chlorophyll and Venus fluorescence channels as well as a merged image. The lower panels show co-localisation of Chl (red) and Venus (yellow) fluorescence intensities over cross-sections of 30-40 cells (with width normalised to 100%) shown as a scatterplot. Brighter red and yellow lines show moving regression curves produced by locally weighted scatterplot smoothing (LOWESS). The histograms show the distribution of the Pearson Correlation Coefficient (PCC) for Chl and Venus fluorescence co-localisation in all cells from three micrographs from individual replicates. A PCC of 1 indicates perfect co-localisation and a PCC of 0 no co-localisation. The cytofluorograms show co-localised Chl and Venus fluorescence intensities as a scatter plot from all cells in three micrographs from independent replicates. Flv4:VN with 30 µM CCCP added in the medium.

No interaction was detected between Flv3:VN and Flv2:VC (Fig. 5c) despite strong expression of both fusion proteins (Supplementary Fig. 3), supporting the notion that Flv2 and Flv3 are unable to form heterooligomers *in vivo*[11], as well as providing a negative control for the observed interactions.

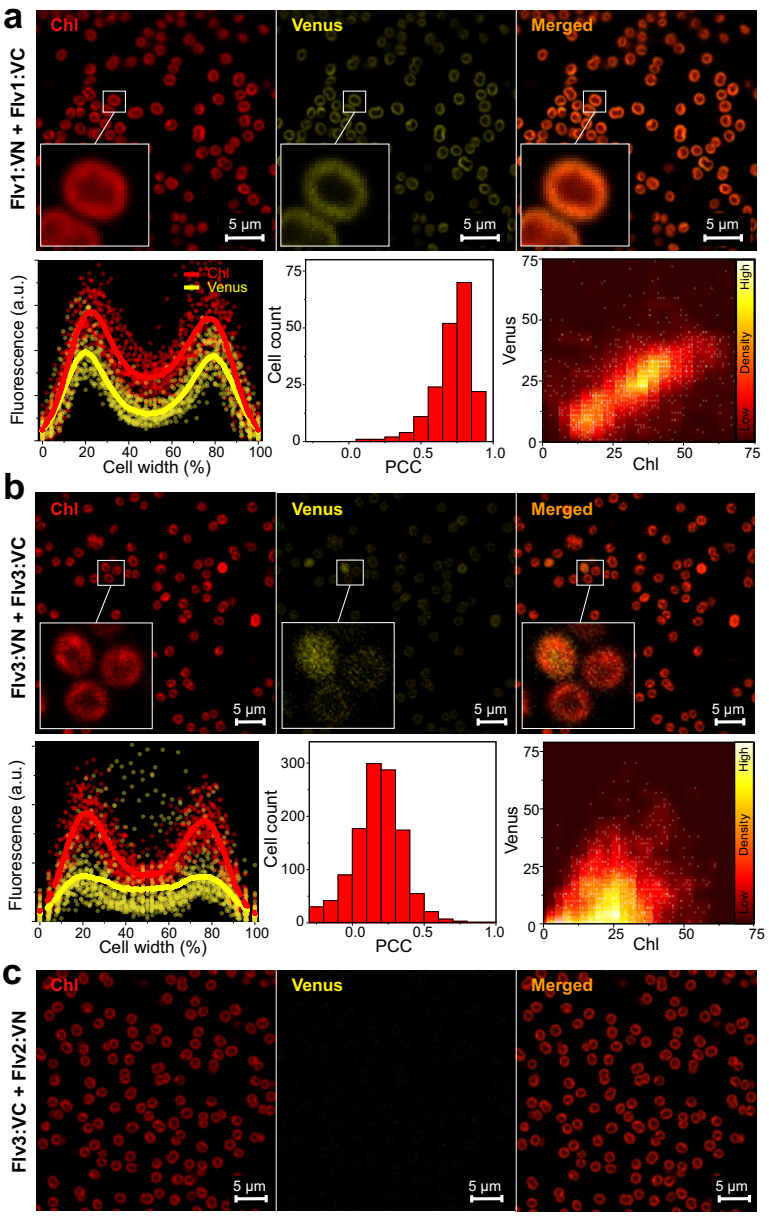

Fig. 5. BiFC tests for Flv1 (A) and Flv3 self-interactions (B) and between Flv2 and Flv3 (C). For details see legends for Fig.s 3 and 4.

Surface charge modelling supports pH-dependent association of FDP heterooligomers with the thylakoid membrane

Lastly, we examined the molecular mechanism underlying the *pmf*-dependent association of FDP heterooligomers with the thylakoid membrane. At low *pmf*, low pH on the cytosolic side of the thylakoid membrane may cause protonation of acidic residues in proteins, giving them a more positive surface charge and promoting electrostatic interactions with negatively charged membrane lipids, or possibly with another protein or a protein complex in the membrane[38,39]. To test this hypothesis, we modelled the electrostatic surface potentials of FDP monomers and oligomers at

different physiologically relevant pH values. In cyanobacteria, cytosolic pH ranges between 7 in dark or low light and 8.5 under strong illumination, also depending on extracellular pH[40,41].

Our analysis revealed that at pH 7.0, Flv1 and Flv3 core monomers have net surface charges of -3.0 ± 0.2e and -11.5 ± 0.6e, respectively. In contrast, at a more alkaline pH of 8.5, the net surface charges decrease to -9.3 ± 0.6e for Flv1 and -18.5 ± 1.1e for Flv3 (Supplementary Figure 12a, c). Similarly, Flv1 core homodimers have a small negative net charge of 3.1 ± 0.8e, with positively charged patches at neutral pH. Those positive patches remain even at alkaline pH, when the Flv1 core homodimer has a negative net charge of -18.9 ± 1.2e, allowing interactions with the membrane, albeit with lower affinity (Figure 6a). The Flv3 core homodimer carries a negative net charge of -12.4 ± 1.9e at pH 7.0, which decreases as low as -29.8 ± 0.8e at pH 8.5 (Figure 6b). Flv1/3 core heterooligomers have a net charge of -11.4 ± 1.6e, with positively charged patches that likely permit interaction with negatively charged membrane lipids. At pH 8.5, the Flv1/3 heterooligomer becomes highly negatively charged (-25.9 ± 1.5e), making membrane interactions unfavourable due to electrostatic repulsion (Figure 6c).

Monomeric Flv2 and Flv4, in turn, carry contrasting net charges. While Flv2 has a highly negative net charge at both pH 7.0 and 8.5 (-16.2 ± 0.4e and -24.2 ± 0.8e), Flv4 monomers have a positive surface charge (+5.8 ± 0.1e) at pH 7.0 and a slightly negative charge (-2.2 ± 0.2e) with large positive patches at pH 8.5 (Supplementary Figure 12b, d). The Flv2/Flv4 heterooligomer has a mostly negative charge of -7.2 ± 0.1e at pH 7.0. However, the positive net charge of Flv4 likely enables interaction with the thylakoid membrane, while at pH 8.5, interaction with a negatively charged membrane surface becomes compromised due to a highly negative net charge of -26.1 ± 0.8e (Figure 6d).

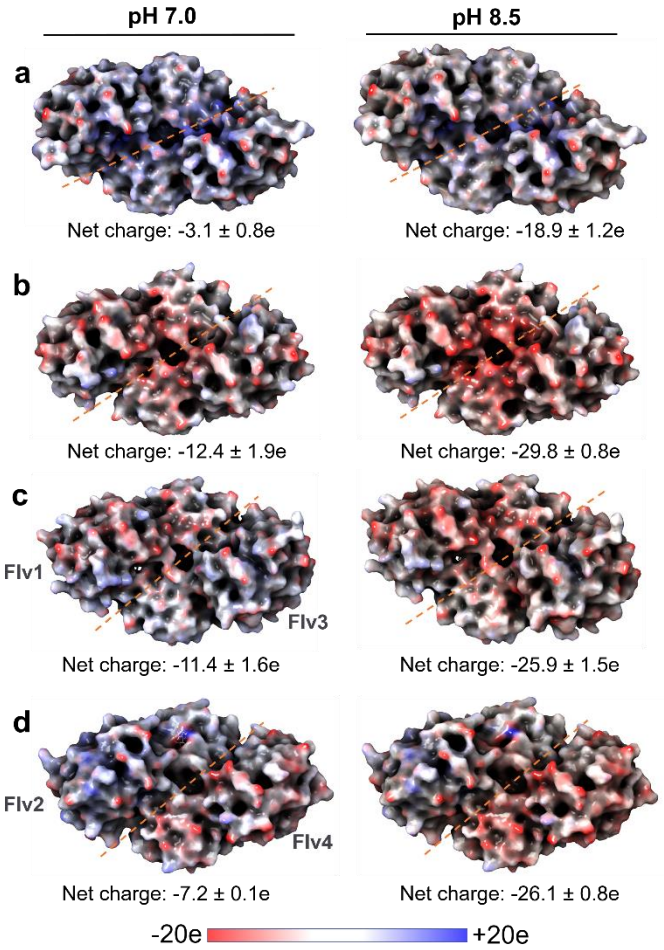

Fig. 6. *In silico* analysis of the electrostatic surface of FDP oligomers at different pH. (a) Flv1/Flv1 homodimer, (b) Flv3/Flv3 homodimer, (c) Flv1/Flv3 heterodimer, and (d) Flv2/Flv4 heterodimer. Surface charges are color-coded with red representing negatively charged regions, blue depicting positively charged regions, and white showing neutral regions. The left panels show a charge at pH 7.0, while the right panels depict a charge at pH 8.5. Since the relative orientation of the C-terminal Flavin reductase domain could not be modelled reliably, only core domains (β-lactamase-like and Flavodoxin-like domains) are shown for visualisation purposes. The orange line indicates the symmetry axis between monomers.

DISCUSSION

Light-dependent reduction of O_2 to H_2O by FDPs, known as the Mehler-like reaction, constitutes a vital, strictly regulated outlet for excessive electrons in the PETC during fluctuations in environmental conditions[3,35,42]. Photosynthetic microorganisms are increasingly employed as green cell factories for sustainable bioproduction of desired compounds, and a thorough understanding of the regulatory mechanisms of photosynthesis is crucial for optimising the absorbed-light-energy-to-product conversion rate in those platforms[43]. In recent years, it has become evident that FDPs can take several homo- and heterooligomeric conformations, but heterooligomers consisting of Flv1 and Flv3 as well as Flv2 and Flv4 are required for the Mehler-like reaction under air-level [CO_2] in *Synechocystis*[10,11]. Several key aspects of this essential regulatory mechanism of photosynthesis,

however, have remained unclear. A) What is the electron donor to FDPs, and does the donor differ between different homo- and heterooligomeric conformations? B) What kind of oligomers can FDPs form and how do they localise within the cell? C) How is the activity of the Mehler-like reaction controlled? An experimental approach combining a BiFC system to visualise protein–protein interactions, biophysical characterisation of photosynthetic electron transport in *Synechocystis* mutant strains, and *in silico* surface charge modelling allowed us to address these questions in the present study. First, we identified *in vivo* interactions between Fed1 and FDPs and confirmed Fed1 as the primary electron donor to both Flv1/3 and Flv2/4 heterooligomers. We also showed that the subcellular localisation differs between different FDP/FDP and FDP/Fed1 interactions, and finally, that the association of Flv1/3 and Flv2/4 interactions with the thylakoid membrane depends on the trans-thylakoid proton gradient (*pmf*), suggesting a feedback mechanism to dynamically control the activity of the Mehler-like reaction.

Previous studies have shown NAD(P)H to be able to donate electrons to recombinant Flv1 or Flv3[2,12] as well as to Flv4[13] *in vitro*. Flv1 and Flv3 monomers or homooligomers cannot catalyse the Mehler-like reaction *in vivo*, however[11], and in this study we demonstrated that severe impairment of light-induced $NADP^+$ reduction in the ΔFNR_L mutant does not significantly decrease FDP photoreduction activity (Fig. 1a-c). The slight decrease that we observed (Fig. 1c) was most likely due to a diminished content of Flv2 in the mutant (Fig. 1d), as lack of Flv2/4 does partially impair the Mehler-like reaction under air level [CO_2][10]. These results indicate that neither NADPH nor FNR can be the main electron donor to the Mehler-like reaction catalysed by Flv1/3 and Flv2/4 heterooligomers.

However, we did observe a protein-protein interaction between FNR_L and Flv3 that strictly localised to the thylakoid membrane (Fig. 1e). The MIMS results suggest that the interaction does not occur due to FNR_L functioning as an electron donor to Flv1/3 heterooligomers. Instead, considering no interaction was observed between FNR_L and Flv1, FNR_L may interact with Flv3 homooligomers to perform an unknown physiological function on thylakoids, or possibly associated with the phycobilisomes, to which FNR binds in cyanobacteria[44]. While Flv3 homooligomers do not catalyse the Mehler-like reaction, overexpression of Flv3 in ΔFlv1 mutant background does partially rescue the growth phenotype of ΔFlv1 in fluctuating light[11], suggesting some non-Mehler-like reaction-related photoprotective function for Flv3 homooligomers. Considering the *in vitro* electron transfer from NADPH to recombinant Flv3, it is possible that NADPH could donate electrons to Flv3 homooligomers, possibly facilitated by the homooligomers interacting directly with FNR_L. We also cannot exclude the possibility of a false positive BiFC result between Flv3 and FNR_L due to the proximity of the two overexpressed proteins at the thylakoid membrane. However, the strong Venus fluorescence signal and the near absence of a signal between Flv1 and FNR_L, despite similar proximity and comparable abundance of fusion proteins (Supplementary Fig. 3), suggest that this is unlikely.

Recent *in vivo* studies have suggested Fed as a more likely electron donor to Flv1/3[15,16], and a recombinant class A FDP from the protozoan *Entamoeba histolytica* has been shown to be able to oxidise Fed *in vitro*[45]. Out of the low-abundance Fed isoforms (Fed2-Fed11), Fed2 has been shown to be essential for the photoautotrophic growth of *Synechocystis*[18]. However, Fed2 functions in low-iron response instead of photosynthetic electron transfer[46], and is unlikely to be a primary electron

donor to FDPs. Fed7, 8, and 9, in turn, have been proposed to function in a stress response pathway in cooperation with the thioredoxin system[21,47], and Fed9 was more recently shown to be important for photomixotrophic growth of *Synechocystis*, likely donating electrons to pyruvate:ferredoxin oxidoreductase (PFOR)[19]. Bacterial-type low-abundance ferredoxins are thus unlikely to constitute the main source of electrons for the light-induced Mehler-like reaction, despite the two-hybrid interaction reported between Fed9 and Flv3[18]. Accordingly, we detected no major impairment of the Mehler-like reaction in any of the mutant strains lacking Fed2-Fed11 (Fig. 2, Supplementary Fig. 4, Supplementary Fig. 5). Using the BiFC system, we showed here that Fed1 interacts *in vivo* with Flv1, Flv3, as well as Flv2 (Fig. 3). Although we cannot exclude minor or redundant roles for low-abundance Feds such as Fed9, these results pinpoint Fed1 as the main electron donor to FDP heterooligomers.

Flv1/Fed1 and Flv3/Fed3 interactions showed contrasting subcellular localisations, as Flv1 interacted with Fed1 at the thylakoids and Flv3 mostly in the cytosol (Fig. 3). Due to strong expression of the fusion proteins (Supplementary Fig. 3), the size of the Flv3 pool in Fed1:VN+Flv3:VC cells substantially exceeds that of Flv1, likely causing a large proportion of Flv3:VC proteins to form homooligomers. The opposite is true in Fed1:VC+Flv1:VN cells. This would suggest that Flv1 homooligomers localise to the thylakoids and Flv3 homooligomers to the cytosol. However, in a majority of cells Flv3 self-interactions (Fig. 5b) as well as Flv3-FNR_L interactions (Fig. 1e) localised to the thylakoids, and the thylakoidal Flv3 self-interaction signals intensified in high concentrations of Ca^{2+} and Mg^{2+} cations (Supplementary Fig. 11). These results suggest that formation of Flv3 homooligomers and/or their association with the thylakoids and FNR may be controlled by the physiological state of the cell, while Flv1 homooligomers consistently associate with the thylakoid membrane. These observations were supported by modelling of surface charges, showing that Flv1 homooligomers carry a low net negative charge with large positively charged patches that likely allow interaction with the thylakoid membrane, while the net surface charge of Flv3 homooligomers was highly negative, making their affinity to negatively charged surface of the thylakoid membrane[48] low (Supplementary Fig. 12). It is clear, however, that further studies are required to elucidate the physiological roles of FDP homooligomers. There also appears to be variation between different cyanobacterial species regarding formation of FDP oligomers and their physiological significance. Our recent study with the filamentous cyanobacterial model species *Anabaena* sp. PCC 7120 revealed that while vegetative cell specific Flv1A and Flv3A likely form heterooligomers and function similarly to their *Synechocystis* orthologues, Flv3A on its own is able to contribute to the Mehler-like reaction and photoprotection of PSI via an unknown mechanism that requires the presence of Flv2 and Flv4[49]. This suggests the existence of functional oligomers consisting of Flv3 and Flv2/4 or possibly interaction of Flv3 homooligomers with Flv2/4 heterooligomers in vegetative *Anabaena* cells. In line with a previous biochemical analysis[11], we detected no interaction between Flv3 and Flv2 in *Synechocystis* (Fig. 5c), but it remains to be confirmed whether such interactions or "exotic" heterooligomerisation occur in *Anabaena* or other cyanobacterial species.

Importantly, the addition of the *pmf*-uncoupling ionophore CCCP to the medium resulted in increased thylakoid localisation of Flv1/3 and, albeit to lesser extent, Flv2/4 interactions (Fig. 4), and increased the maximal light-induced O_2 uptake rate relative to O_2 evolution (Supplementary Fig. 9). Under air-level [CO_2], the strong O_2 photoreduction catalysed by Flv1/3 heterooligomers

occurs transiently at the dark-light transition or upon sudden increases in light intensity, providing an outlet for excessive electrons in the PETC[10]. The transience of this reaction suggests reversible post-translational regulation of Flv1/3 activity, and several putative mechanisms, such as a redox regulation by the thioredoxin system or phosphorylation and de-phosphorylation have been proposed[35,42]. Our findings in the current study suggest that FDP heterooligomers are amphitropic: the magnitude of the *pmf* regulates their activity by determining whether they associate with the thylakoid membrane. As we have previously shown that up to 75% of *pmf* generation during dark-to-light transitions is dependent on FDP-catalysed O_2 photoreduction in *Synechocystis*[15], we propose a self-regulatory feedback loop. In darkness or immediately after a dark-light transition, *pmf* is low and cytosolic pH close to neutral, allowing FDP heterooligomers to localise at the thylakoid membrane and catalyse strong reduction of O_2 upon illumination (Fig. 7a). This occurs when CO_2 fixation has not been yet fully activated, and, due to *pmf* being low, photosynthetic control at Cytochrome b6f is not limiting electron transport to PSI. As a result, the presence of a strong FDP electron sink becomes central for photoprotection. The high rate of O_2 photoreduction elevates the *pmf* directly by consuming protons on the cytosolic side of the membrane and indirectly by keeping the Fed1 pool oxidised, thereby allowing a higher electron transport rate in the PETC. The higher *pmf* then causes Flv1/3 heterooligomers to disassociate from the thylakoids, decreasing their O_2 reduction activity (Fig. 7b). In this manner, high Flv1/3 activity during the first minute of illumination would result in downregulation of Flv1/3 activity after the initial peak. This is exactly what we have previously reported: O_2 photoreduction peaks after c.a. 20-30 seconds of strong illumination, which is also when a steady-state level of *pmf* is reached in WT cells[15]. After 30 seconds, the rate of O_2 photoreduction declines, especially in low [CO_2] grown cells or under alkaline pH (when *Flv2* and *Flv4* are not expressed)[10].

It has been reported previously that Flv2 and Flv4 are in the thylakoid fraction when *Synechocystis* proteins are extracted in a buffer containing high concentrations of Mg^{2+} and Ca^{2+} cations, and in the soluble fraction when extracted in a cation-depleted buffer [14]. *Pmf* generation was delayed during dark-to-light transitions in low cation in comparison to high cation medium (Supplementary Fig. 7), but likely due to impairment of the function of unknown cation channels or antiporters on the thylakoid membrane[50], resulting in diminishment of initial $\Delta\psi$ (electric potential component of *pmf*). However, we detected no difference in the subcellular localisation of Flv2/4 interactions between low and high cation media (Supplementary Fig. 8b). These observations suggest that the loss of the ΔpH component of *pmf*, specifically, promotes the thylakoid association of FDP heterooligomers. For example, in plant chloroplasts low stromal pH promotes the binding of FNR to its membrane anchor Tic62[51].

Indeed, *in silico* modelling revealed that the molecular mechanism underlying the reversible association of FDP heterooligomers with the thylakoid membrane depends on changes in net surface charges within a physiological pH range (Fig. 6). In neutral cytosolic pH such as in dark or low light conditions, Flv1/3 and Flv2/4 heterooligomers maintain low negative net charge with positive patches that enable interaction with membrane lipids or positively charged membrane proteins. In contrast, at higher pH mimicking the alkalisation of the cytosol upon strong illumination, the net charges of FDP heterooligomers become highly negative, repelling them from the membrane. As the cytosol gradually gets more alkaline under illumination (Supplementary Fig. 10), the positive net charge of Flv4 (Fig. 6) may allow Flv2/4 heterooligomers to remain bound to

the membrane longer than Flv1/3 heterooligomers (Fig. 7b-c). This could explain the distinct kinetics of Flv1/3 and Flv2/4-mediated O_2 photoreduction, where Flv1/3 catalyses a strong but transient reaction, and Flv2/4 a more sustained O_2 photoreduction further into dark-light transitions[10].

The proposed pH-dependent regulatory mechanism of FDP activity may also indirectly control the induction of the carbon concentrating mechanism (CCM), as at least in algae, CCM induction was recently shown to depend on *pmf* generation by FDPs and CET[52]. Our recent results with Anabaena suggest that a similar dependency may also exist in cyanobacteria[49].

In conclusion, the present study elucidates the regulation of the Mehler-like reaction and advances our understanding of how photoprotective mechanisms are orchestrated in dynamic, natural light environments. Our findings confirm Fed1 as the primary electron donor for the reaction catalysed by FDP heterooligomers. Furthermore, we demonstrate that the activity of the Mehler-like reaction is regulated by reversible association with the thylakoid membrane via pH-dependent changes in electrostatic surface charges of FDP heterooligomers. We propose a model of a self-regulatory feedback mechanism that controls the activity of the Mehler-like reaction. Our model posits that the Mehler-like reaction, by being crucial for generation of *pmf* upon increases in light intensity, promotes its own inactivation by *pmf*-induced disassociation from the thylakoid membrane. This ensures that the Mehler-like reaction is downregulated in order not to waste energy when a release valve for excessive electrons in the PETC is not needed. By shedding light on the intricate mechanisms that optimise photosynthetic efficiency, our study provides a foundation for rationally directing electron flux toward desired reactions in photosynthesis-based biotechnological applications.

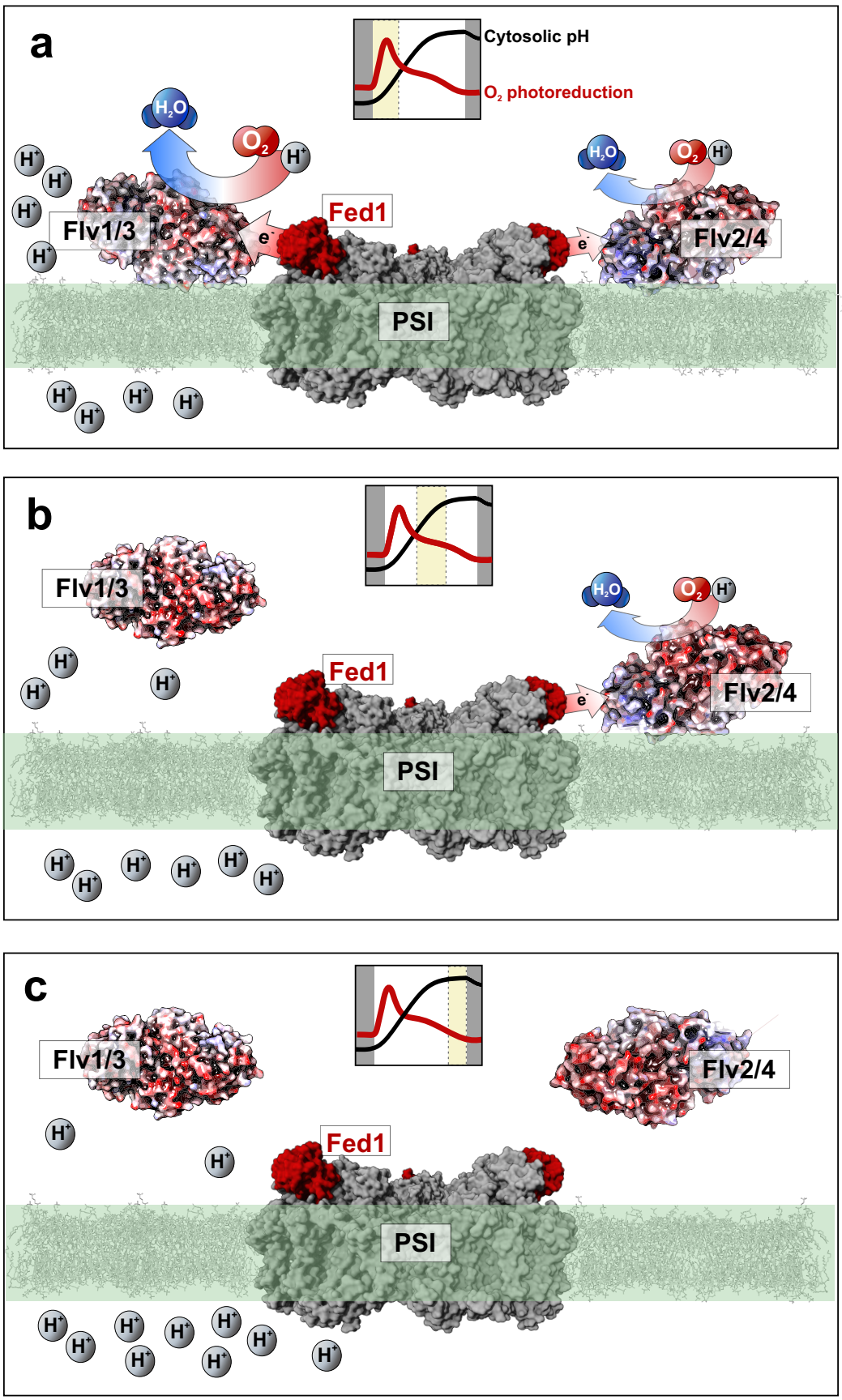

Fig. 7. Schematic model for pH-dependent association of FDP heterooligomers with the thylakoid membrane. (a) In dark or shortly after a dark-light transition, when *pmf* is low and cytosolic pH close to neutral, a more positive surface charge of FDP heterooligomers allows them bind to the thylakoid membrane and catalyse strong Mehler-like reaction using electrons from reduced Fed1. (b) As *pmf* rises and the cytosol

becomes increasingly alkaline, Flv1/3 heterooligomers are repelled from the membrane due to their surface charges becoming more negative. This inhibits Flv1/3 activity and results in the decline of the O_2 photoreduction rate. Due to the positive charge of Flv4, however, Flv2/4 heterooligomers still maintain affinity to the thylakoid membrane, catalysing residual O_2 photoreduction. (c) When the cytosol becomes highly alkaline upon full activation of CO_2 fixation, both FDP heterooligomers disassociate from the thylakoids, strongly inhibiting (now unnecessary) O_2 photoreduction activity. Trimeric PSI structure with bound Fed is based on[53.] The small inlets within each panel represent typical kinetics of O_2 photoreduction in red, and alkalisation of the cytosol (see Supplementary Fig. 10b) in black during a dark-to-light transition. The yellow rectangles indicate the phase depicted in the panel.

METHODS

Creation of *Synechocystis* BiFC strains

BiFC is prone to false positive results, especially when examining interactions of overexpressed proteins in a small compartment such as a cyanobacterial cell[24]. To ameliorate this disadvantage, we used a Venus YFP variant where a I152L mutation in the N-terminal fragment decreases the propensity of the two fragments to self-reassemble, substantially decreasing the number of false positives[54]. Proteins of interest were fused to the N or C terminal Venus-fragment via a short linker sequence to allow increased flexibility. We co-expressed the fusion proteins under IPTG-inducible lac2 promoters and S3 ribosome binding sites (RBS) of the *cpcB* gene (encoding the phycocyanin subunit β) from a single pDF-lac2 plasmid [55]. RBS S3 has been shown to enable strong expression of YFP[55].

The *Synechocystis* sp. PCC6803 coding sequences of *flv1* (sll1521), *flv2* (sll0219), *flv3* (sll0550), *flv4* (sll0217), *petF* (sll0020), *petH* (slr1643) full sequence coding for FNR_L, and *petH* nucleotides 337–1242 coding for FNR_S ,as well as N-terminal (VN; nucleotides 1–468) and C-terminal (VC; nucleotides 469–724) fragments of the Venus I152L variant [54] were synthetized by GenScript (Piscataway, NJ, USA). In all cases a CAT codon coding for an extra Histidine residue was added to the sequences after the first ATG start codon in order to generate NsiI restriction sites (ATGCAT) at 5´ ends of the constructs. The 3´ stop codons were removed and chloramphenicol resistance (Cm^R) cassettes with an NheI site at the 5´end and an NheI as well as a XhoI site at the 3´end were added. For *flv3*, a synonymous A1579T mutation was introduced to remove an endogenous NheI restriction site. SpeI restriction sites (ACTAGT) as well as flexible short linker sequences (CTGCCGGGCCCGGAGCTGCCG) were added at the 5´ends of the Venus fragments, while CmR cassettes flanked by NheI sites and followed by a SalI site (GTCGAC) were added at the 3´ ends. All *Synechocystis* gene sequences were retrieved from the CyanoBase database[56].

A modular cloning strategy as described in[55] was then used to assemble the gene-VN/VC expression vectors in the pDF-lac2 plasmid. First, the synthesised gene-Cm^R fragments were subcloned as NsiI-XhoI fragments downstream of a S3 RBS in pNiv carrier plasmids. The plasmid was then cleaved with NheI and XhoI, removing the Cm^R. A VN- or VC-Cm^R fragment was inserted in frame to the 3’ of the first gene by SpeI/SalI cloning. The resultant pNiv-S3-gene 1-VN/VC-Cm^R plasmid was then cut with NheI/SalI and a S3-gene 2-VN/VC-Cm^R construct was

inserted as a SpeI/SalI fragment downstream of the gene 1-VN/VC construct in the pNiv-S3 plasmid. Finally, constructs containing the two genes fused to VC or VN were transferred as SpeI/SalI fragments into pDF-lac2 expression plasmids.

Wild-type *Synechocystis* sp. PCC 6803 cells were then transformed with the generated pDF-lac2 constructs (Supplementary Fig. 13). Transformants were selected on BG-11 plates containing increasing concentrations of chloramphenicol and spectinomycin, up to 35 and 50 µg/ml, respectively. The presence of the transgenes in the strains was verified by PCR using primers against on the 5' side (TGAGCGGATAACAATTTCACACAGAATT) and the 3' side of the cloning site in pDF-lac2 (GACCGCTTCTGCGTTCTGATTTAAT).

Other strains and culture conditions

We used the glucose-tolerant *Synechocystis* sp. PCC 6803 WT strain[57], mutant strains ΔFed2/Fed2, ΔFed3, ΔFed4, ΔFed5/Fed5, ΔFed6, ΔFed7Fed8Fed9, ΔFed9[19], the ΔFlv3 strain[9], as well as the ΔFNR_L (FSI) and ΔFNR_S (MI6) strains, deficient in the large and small isoform of FNR, respectively[29]. To create the ΔFed10 and ΔFed11 mutants, three fragments of the *Fed10* (sll1584) and *Fed11* (ssl3044)[17] genes were amplified by PCR. These were the respective up- (primer 1 and 2) and downstream (primer 5 and 6) regions as well as the kanamycin antibiotic resistance cassette (primer 3 and 4) (Supplementary Table 1). Subsequently, constructs were generated by Gibson cloning[58], assembling the three fragments into the pBluescript SK(+) vector in a single step. After sequencing the plasmids were transformed into *Synechocystis* sp. PCC 6803 cells as described[57]. Resulting transformants were checked by PCR after several rounds of segregation (Supplementary Fig. 4a).

Pre-experimental cultures and the *Synechocystis* BiFC strains were grown in 30 ml of BG-11 medium pH 7.5 with agitation under 3% [CO_2] at 30ºC under continuous illumination of white light of 50 µmol photons $m^{-2}s^{-1}$. Mutant pre-cultures were supplemented with appropriate antibiotics. Cells were harvested at the logarithmic growth phase and re-suspended in fresh BG-11 without antibiotics at OD_{750}=0.2. Cultures were then moved to air [CO_2] / 30ºC and illuminated continuously with white light at 50 µmol photons $m^{-2}s^{-1}$.

Membrane-inlet mass spectrometry

Exchange of $^{16}O_2$ (*m/z*=32) and $^{18}O_2$ (*m/z*=36) was measured *in vivo* with membrane-inlet mass spectrometry (MIMS) as described in [11]. After harvesting, cells were resuspended in fresh BG-11 pH 7.5, adjusted to 10 µg Chlorophyll (Chl) *a* ml^{-1}, and kept for one hour in air [CO_2] under 50 µmol photons $m^{-2}s^{-1}$. Cells were supplemented with $^{18}O_2$ at an equivalent concentration to $^{16}O_2$ and with 1.5 mM $NaHCO_3$, and dark-adapted for 15 min, after which O_2 exchange was monitored during a 5 min period of illumination with 500 µmol photons $m^{-2}s^{-1}$ of white actinic light. O_2 exchange rates were calculated as described by[59].

Bimolecular fluorescence complementation (BiFC) tests

The BiFC strains were grown in BG-11 pH 7.5 supplemented with 35 µg/ml of chloramphenicol and 50 µg/ml of spectinomycin under 3% [CO_2] at 30°C under continuous illumination of 50 µmol photons $m^{-2}s^{-1}$ of white light until OD_{750} was c.a. 0.5. OD_{750} was then adjusted to 0.25 with standard fresh BG-11 pH 7.5 without antibiotics, BG-11 without added sources of Mg^{2+} or Ca^{2+} cations, or BG-11 supplemented with 25 mM $MgCl_2$ and 30mM $CaCl_2$. Cultures were supplemented with 1 mM IPTG to induce expression of the BiFC fusion proteins. Cultures were then grown overnight in the same conditions as before, harvested, and resuspended in 2 ml of similar BG-11 pH as above. Finally, Venus fluorescence and chlorophyll autofluorescence from the cells were imaged with an Zeiss LSM880 laser-scanning confocal microscope using a 63x or 100x objective with excitation at 488 and 543 nm, and detection at 518–621 nm. 30 µM CCCP was added to the cell suspensions before imaging when appropriate. Quantification of Venus and Chl fluorescence co-localisation was performed using the EzColocalization plugin for the Fiji software[60]. Costes' threshold was used to calculate the Pearson correlation coefficient.

NADPH fluorescence changes

NADPH fluorescence changes between 420 and 580 nm were monitored with a Dual-PAM 100 spectrophotometer and its 9-AA/NADPH accessory module (Walz)[61]. Cells were harvested, resuspended in fresh BG-11 and adjusted to 5 µg Chl *a* ml^{-1}. Cells were dark-adapted for 15 min prior to measurement of NADPH fluorescence changes under 500 µmol photons $m^{-2}s^{-1}$ illumination for 40 s, followed by 30 s in darkness.

Near-infrared spectrophotometry

In vivo redox changes of P700, PC, and Fed were deconvoluted from absorbance differences at four near-infrared (NIR) wavelength pairs at 780–820, 820–870, 840–965 and 870–965 nm measured with a DUAL-KLAS-NIR spectrophotometer (Walz). The differential model plot (DMP) used to deconvolute the Fed signal was determined from ΔFlv3 D1D2 triple mutant cells as described in[15], while the P700 and PC DMPs were determined as described by[32]. Cells were grown as for the BiFC tests, harvested, resuspended in fresh BG-11 and adjusted to 20 µg Chl *a* ml^{-1}. Cells were dark-adapted for 15 min prior to measurement. We used the NIRMAX script[62] consisting of a 3 s illumination with strong AL (1750 µmol photons m^{-2} sec^{-1}), with a saturating pulse after 200 ms of illumination to fully reduce the Fed pool. After 4 s of darkness, cells were illuminated under far red (FR) light for 10 s with a saturating pulse at the end to fully oxidise P700 and PC. The maximum reduction values of Fed and maximum oxidation values of P700 and PC thus obtained were used to normalise the traces.

Electrochromic shift (ECS) measurements

Light-induced changes in the *pmf*, thylakoid conductivity (gH+) and thylakoid proton flux (vH+) were determined by monitoring the dark interval relaxation kinetics (DIRK) of the absorbance

difference between 500 and 480 nm, which constitutes the ECS in *Synechocystis*[36], as described previously[15]. Cells were harvested and resuspended in fresh BG-11, low cation BG-11, or high cation BG-11 (see above) pH 7.5 at a Chl concentration of 7.5 µg/ml. Suspensions were illuminated at 500 µmol photons $m^{-2}s^{-1}$ with 600 ms dark intervals as indicated in the Fig. legends, and 500-480 nm absorbance changes were detected using a JTS-10 spectrophotometer (BioLogic) and appropriate interference filters (Edmund Optics).

Acridine orange (AO) and acridine yellow (AY) fluorescence measurements

To monitor the light-induced alkalisation of the cytosol, AO and AY fluorescence changes[37] were recorded using a Dual-PAM-100 spectrophotometer and the AO/AY emitter-detector module[61]. Cells were grown in air level CO2 in BG-11 pH 7.5 under 50 µmol photons $m^{-2}s^{-1}$ for four days, harvested, and suspended in fresh BG-11 with Chl concentration adjusted to 5 µg/ml. 5 µM AO or AY, and 1mM KCN (when appropriate) was added before a 10 min dark-adaptation prior to measurements under 500 µmol photons $m^{-2}s^{-1}$.

Immunoblotting

Total proteins were extracted from BiFC cultures used for microscopy as described by[63], separated by sodium dodecyl sulphate (SDS) polyacrylamide gel electrophoresis on 12% gels with 6M urea and transferred to polyvinylidene fluoride membranes. Membranes were probed with primary antibodies against the N-terminal fragment of YFP (Origene), Flv2 and Flv3 (Antiprot), and PetH (kindly shared by H. Matthijs). Horseradish peroxidase (HRP) -conjugated goat-anti mouse (Bio-Rad) and goat-anti-rabbit (GE Healthcare) secondary antibodies as well as ECL (Amersham) were used for detection.

In silico modelling of protein surface charges

The sequences of *Synechocystis* sp. PCC 6803 Flv1 (sll1521), Flv2 (sll0219), Flv3 (sll0550), and Flv4 (Sll0217) proteins were retrieved from UniProt using the following IDs: P74373, P72723, Q55393, and P72721, respectively. The crystal structures for the multiple structure-based alignments were retrieved by BLAST searches from the Protein Data Bank[64] using these FDP sequences as queries. The 3D models for the open and closed state of the core composed of β-lactamase-like and flavodoxin domains of Flv1, Flv2, Flv3, and Flv4 monomers, as well as Flv1/Flv1 and Flv3/Flv3 homooligomers, and Flv1/Flv3 and Flv2/Flv4 heterooligomers were built based on the alignment and the crystal structure of $F_{420}H_2$ oxidase from the methanogenic archaea *Methanothermobacter marburgensis* (PDB IDs: 2OHI for closed conformation and 2OHJ for open conformation)[65] using MODELLER v.10.4[66]. The N-terminal and C-terminal domains of the Flv1 and Flv3 flavodiiron core were aligned separately to achieve optimal alignment. For C-terminal flavin reductase domain modelling, the crystal structure of *Thermus thermophilus* putative flavoprotein (PDB ID: 1WGB) was used as a template. Then, monomeric models were overlaid with dimeric *E. coli* FLRD protein[67]. Full-size homo- and heterooligomers were constructed

through multiple-template modelling in MODELLER using the earlier constructed core and flavin reductase domain models as templates. In all cases, ligands and structural waters have been directly transferred from the templates during modelling. The models with the lowest zDOPE and Molpdf scores were selected for further analysis. Following protein preparation at pH 7.0 and pH 8.5 using the "prepwizard" script, the net charges were calculated in triplicate using the "calc_protein_descriptors" script in Schrodinger Bioluminate[68]. The electrostatic potential surfaces for FDP monomers and oligomers were visualised with the Poisson-Boltzmann ESP module in Schrodinger Maestro[69].

Data availability

All relevant data are included in the figures, the Supplementary Information, and the Source Data. Raw microscopy images are available from the corresponding author upon reasonable request.

REFERENCES

1. Allahverdiyeva, Y., Isojärvi, J., Zhang, P. & Aro, E.-M. Cyanobacterial Oxygenic Photosynthesis is Protected by Flavodiiron Proteins. *Life (Basel)* **5**, 716–743 (2015).

2. Vicente, J. B., Gomes, C. M., Wasserfallen, A. & Teixeira, M. Module fusion in an A-type flavoprotein from the cyanobacterium *Synechocystis* condenses a multiple-component pathway in a single polypeptide chain. *Biochem Biophys Res Commun* **294**, 82–87 (2002).

3. Allahverdiyeva, Y. *et al.* Flavodiiron proteins Flv1 and Flv3 enable cyanobacterial growth and photosynthesis under fluctuating light. *Proc Natl Acad Sci U S A* **110**, 4111–4116 (2013).

4. Chaux, F. *et al.* Flavodiiron Proteins Promote Fast and Transient O-2 Photoreduction in Chlamydomonas. *Plant Physiol* **174**, 1825–1836 (2017).

5. Gerotto, C. *et al.* Flavodiiron proteins act as safety valve for electrons in Physcomitrella patens. *Proc Natl Acad Sci U S A* **113**, 12322–12327 (2016).

6. Folgosa, F., Martins, M. C. & Teixeira, M. Diversity and complexity of flavodiiron NO/O2 reductases. *FEMS Microbiol Lett* **365**, (2018).

7. Burlacot, A., Richaud, P., Gosset, A., Li-Beisson, Y. & Peltier, G. Algal photosynthesis converts nitric oxide into nitrous oxide. *Proc Natl Acad Sci U S A* **117**, 2704–2709 (2020).

8. Blomberg, M. R. A. & Ädelroth, P. Reduction of Nitric Oxide to Nitrous Oxide in Flavodiiron Proteins: Catalytic Mechanism and Plausible Intermediates. *ACS Catal* **13**, 2025–2038 (2023).

9. Helman, Y. *et al.* Genes encoding a-type flavoproteins are essential for photoreduction of O-2 in cyanobacteria. *Current Biology* **13**, 230–235 (2003).

10. Santana-Sanchez, A. *et al.* Flavodiiron proteins 1-to-4 function in versatile combinations in O-2 photoreduction in cyanobacteria. *Elife* **8**, e45766 (2019).

11. Mustila, H. *et al.* The Flavodiiron Protein Flv3 Functions as a Homo-Oligomer During Stress Acclimation and is Distinct from the Flv1/Flv3 Hetero-Oligomer Specific to the O-2 Photoreduction Pathway. *Plant Cell Physiol* **57**, 1468–1483 (2016).

12. Brown, K. A. *et al.* The oxygen reduction reaction catalyzed by *Synechocystis* sp. PCC 6803 flavodiiron proteins. *Sustain Energy Fuels* **3**, 3191–3200 (2019).

13. Shimakawa, G. *et al.* FLAVODIIRON2 and FLAVODIIRON4 Proteins Mediate an Oxygen-Dependent Alternative Electron Flow in *Synechocystis* sp PCC 6803 under CO2-Limited Conditions. *Plant Physiol* **167**, 472-U732 (2015).

14. Zhang, P. *et al.* Operon flv4-flv2 Provides Cyanobacterial Photosystem II with Flexibility of Electron Transfer. *Plant Cell* **24**, 1952–1971 (2012).

15. Nikkanen, L. *et al.* Functional redundancy between flavodiiron proteins and NDH-1 in *Synechocystis* sp. PCC 6803. *Plant J* **103**, 1460–1476 (2020).

16. Sétif, P., Shimakawa, G., Krieger-Liszkay, A. & Miyake, C. Identification of the electron donor to flavodiiron proteins in *Synechocystis* sp. PCC 6803 by in vivo spectroscopy. *Biochim Biophysi Acta Bioenergetics* **1861**, 148256 (2020).

17. Artz, J. H. *et al.* The structure and reactivity of the HoxEFU complex from the cyanobacterium *Synechocystis* sp. PCC 6803. *J Biol Chem* **295**, 9445–9454 (2020).

18. Cassier-Chauvat, C. & Chauvat, F. Function and Regulation of Ferredoxins in the Cyanobacterium, *Synechocystis* PCC6803: Recent Advances. *Life (Basel)* **4**, 666–680 (2014).

19. Wang, Y. *et al.* Pyruvate:ferredoxin oxidoreductase and low abundant ferredoxins support aerobic photomixotrophic growth in cyanobacteria. *Elife* **11**, (2022).

20. Hanke, G. T., Satomi, Y., Shinmura, K., Takao, T. & Hase, T. A screen for potential ferredoxin electron transfer partners uncovers new, redox dependent interactions. *Biochim Biophys Acta Proteins Proteom* **1814**, 366–374 (2011).

21. Mustila, H., Allahverdiyeva, Y., Isojarvi, J., Aro, E. M. & Eisenhut, M. The bacterial-type [4Fe-4S] ferredoxin 7 has a regulatory function under photooxidative stress conditions in the cyanobacterium *Synechocystis* sp PCC 6803. *Biochimi Biophys Acta Bioenergetics* **1837**, 1293–1304 (2014).

22. Kerppola, T. K. Bimolecular fluorescence complementation (BiFC) analysis as a probe of protein interactions in living cells. *Annu Rev Biophys* **37**, 465–487 (2008).

23. Hu, C. D., Chinenov, Y. & Kerppola, T. K. Visualization of interactions among bZip and Rel family proteins in living cells using bimolecular fluorescence complementation. *Mol Cell* **9**, 789–798 (2002).

24. Kudla, J. & Bock, R. Lighting the Way to Protein-Protein Interactions: Recommendations on Best Practices for Bimolecular Fluorescence Complementation Analyses. *Plant Cell* **28**, 1002–1008 (2016).

25. Waadt, R. & Kudla, J. In Planta Visualization of Protein Interactions Using Bimolecular Fluorescence Complementation (BiFC). *CSH Protoc* **2008**, pdb.prot4995 (2008).

26. Walter, M. *et al.* Visualization of protein interactions in living plant cells using bimolecular fluorescence complementation. *Plant J* **40**, 428–438 (2004).

27. Nikkanen, L., Toivola, J. & Rintamäki, E. Crosstalk between chloroplast thioredoxin systems in regulation of photosynthesis. *Plant Cell Environ* **39**, 1691–1705 (2016).

28. Yokoo, R., Hood, R. D. & Savage, D. F. Live-cell imaging of cyanobacteria. *Photosynth Res* **126**, 33–46 (2015).

29. Thomas, J.-C., Ughy, B., Lagoutte, B. & Ajlani, G. A second isoform of the ferredoxin:NADP oxidoreductase generated by an in-frame initiation of translation. *Proc Natl Acad Sci U S A* **103**, 18368–18373 (2006).

30. Miller, N. T., Ajlani, G. & Burnap, R. L. Cyclic Electron Flow-Coupled Proton Pumping in *Synechocystis* sp. PCC6803 Is Dependent upon NADPH Oxidation by the Soluble Isoform of Ferredoxin:NADP-Oxidoreductase. *Microorganisms* **10**, 855 (2022).

31. Korn, A., Ajlani, G., Lagoutte, B., Gall, A. & Sétif, P. Ferredoxin:NADP+ Oxidoreductase Association with Phycocyanin Modulates Its Properties. *J Biol Chem* **284**, 31789–31797 (2009).

32. Theune, M. L. *et al.* In-vivo quantification of electron flow through photosystem I – Cyclic electron transport makes up about 35% in a cyanobacterium. *Biochim Biophysi Acta Bioenergetics* **1862**, 148353 (2021).

33. Poncelet, M., Cassier-Chauvat, C., Leschelle, X., Bottin, H. & Chauvat, F. Targeted deletion and mutational analysis of the essential (2Fe-2S) plant-like ferredoxin in *Synechocystis* PCC6803 by plasmid shuffling. *Mol Microbiol* **28**, 813–821 (1998).

34. Gutekunst, K. *et al.* The Bidirectional NiFe-hydrogenase in *Synechocystis* sp. PCC 6803 Is Reduced by Flavodoxin and Ferredoxin and Is Essential under Mixotrophic, Nitrate-limiting Conditions. *J Biol Chem* **289**, 1930–1937 (2014).

35. Nikkanen, L., Solymosi, D., Jokel, M. & Allahverdiyeva, Y. Regulatory electron transport pathways of photosynthesis in cyanobacteria and microalgae: Recent advances and biotechnological prospects. *Physiol Plant* **173**, 514–525 (2021).

36. Viola, S. *et al.* Probing the electric field across thylakoid membranes in cyanobacteria. *Proc Natl Acad Sci U S A* **116**, 21900–21906 (2019).

37. Teuber, M., Rogner, M. & Berry, S. Fluorescent probes for non-invasive bioenergetic studies of whole cyanobacterial cells. *Biochim Biophys Acta Bioenergetics* **1506**, 31–46 (2001).

38. Johnson, J. E. & Cornell, R. B. Amphitropic proteins: regulation by reversible membrane interactions (Review). *Mol Membr Biol* **16**, 217–235 (1999).

39. Mulgrew-Nesbitt, A. *et al.* The role of electrostatics in protein–membrane interactions. *Biochimica et Biophysica Acta (BBA) - Mol Cell Biol Lipids* **1761**, 812–826 (2006).

40. Mangan, N. M., Flamholz, A., Hood, R. D., Milo, R. & Savage, D. F. pH determines the energetic efficiency of the cyanobacterial CO2 concentrating mechanism. *Proc Natl Acad Sci U S A* **113**, E5354–E5362 (2016).

41. Coleman, J. R. & Colman, B. Inorganic Carbon Accumulation and Photosynthesis in a Blue-green Alga as a Function of External pH. *Plant Physiol* **67**, 917–921 (1981).

42. Alboresi, A., Storti, M., Cendron, L. & Morosinotto, T. Role and regulation of class-C flavodiiron proteins in photosynthetic organisms. *Biochem J* **476**, 2487–2498 (2019).

43. Nikkanen, L., Hubacek, M. & Allahverdiyeva, Y. 10 Photosynthetic microorganisms as biocatalysts. in (ed. Rögner, M.) 257–278 (De Gruyter, 2021). doi:doi:10.1515/9783110716979-010.

44. Liu, H. *et al.* Phycobilisomes Harbor FNR $_L$ in Cyanobacteria. *mBio* **10**, (2019).

45. Cabeza, M. S., Guerrero, S. A., Iglesias, A. A. & Arias, D. G. New enzymatic pathways for the reduction of reactive oxygen species in Entamoeba histolytica. *Biochim Biophys Acta General Subjects* **1850**, 1233–1244 (2015).

46. Schorsch, M. *et al.* A unique ferredoxin acts as a player in the low-iron response of photosynthetic organisms. *Proc Natl Acad Sci U S A* **115**, E12111–E12120 (2018).

47. Marteyn, B., Domain, F., Legrain, P., Chauvat, F. & Cassier-Chauvat, C. The thioredoxin reductase-glutaredoxins-ferredoxin crossroad pathway for selenate tolerance in *Synechocystis* PCC6803. *Mol Microbiol* **71**, 520–532 (2009).

48. Barber, J. Influence of Surface Charges on Thylakoid Structure and Function. *Annu Rev Plant Physiol* **33**, 261–295 (1982).

49. Santana-Sánchez, A. *et al.* Flv3A facilitates O_2 photoreduction and affects H_2 photoproduction independently of Flv1A in diazotrophic *Anabaena* filaments. *New Phytol* **237**, 126–139 (2023).

50. Carraretto, L. *et al.* Ion Channels in Plant Bioenergetic Organelles, Chloroplasts and Mitochondria: From Molecular Identification to Function. *Mol Plant* **9**, 371–395 (2016).

51. Benz, J. P. *et al.* Arabidopsis Tic62 and Ferredoxin-NADP(H) Oxidoreductase Form Light-Regulated Complexes That Are Integrated into the Chloroplast Redox Poise. *Plant Cell* **21**, 3965–3983 (2009).

52. Burlacot, A. *et al.* Alternative photosynthesis pathways drive the algal CO2-concentrating mechanism. *Nature* **605**, 366–371 (2022).

53. Li, J. *et al.* Structure of cyanobacterial photosystem I complexed with ferredoxin at 1.97 Å resolution. *Commun Biol* **5**, 951 (2022).

54. Kodama, Y. & Hu, C.-D. An improved bimolecular fluorescence complementation assay with a high signal-to-noise ratio. *Biotechniques* **49**, 793-+ (2010).

55. Thiel, K. *et al.* Redirecting photosynthetic electron flux in the cyanobacterium *Synechocystis* sp. PCC 6803 by the deletion of flavodiiron protein Flv3. *Microb Cell Fact* **18**, 182–189 (2019).

56. Nakamura, Y. CyanoBase, a www database containing the complete nucleotide sequence of the genome of *Synechocystis* sp. strain PCC6803. *Nucleic Acids Res* **26**, 63–67 (1998).

57. Williams, J. G. K. Construction of Specific Mutations in Photosystem-Ii Photosynthetic Reaction Center by Genetic-Engineering Methods in *Synechocystis*-6803. *Methods Enzymol* **167**, 766–778 (1988).

58. Gibson, D. G. *et al.* Enzymatic assembly of DNA molecules up to several hundred kilobases. *Nat Methods* **6**, 343–345 (2009).

59. Beckmann, K., Messinger, J., Badger, M. R., Wydrzynski, T. & Hillier, W. On-line mass spectrometry: membrane inlet sampling. *Photosynth Res* **102**, 511–522 (2009).

60. Stauffer, W., Sheng, H. & Lim, H. N. EzColocalization: An ImageJ plugin for visualizing and measuring colocalization in cells and organisms. *Sci Rep* **8**, 15764 (2018).

61. Schreiber, U. & Klughammer, C. New NADPH/9-AA module for the DUAL-PAM-100: Description, operation and examples of application. *PAM Application Notes* **2**, 1–13 (2009).

62. Klughammer, C. & Schreiber, U. Deconvolution of ferredoxin, plastocyanin, and P700 transmittance changes in intact leaves with a new type of kinetic LED array spectrophotometer. *Photosynth Res* **128**, 195–214 (2016).

63. Zhang, P., Allahverdiyeva, Y., Eisenhut, M. & Aro, E.-M. Flavodiiron Proteins in Oxygenic Photosynthetic Organisms: Photoprotection of Photosystem II by Flv2 and Flv4 in *Synechocystis* sp PCC 6803. *PLoS One* **4**, e5331 (2009).

64. Berman, H. M. The Protein Data Bank. *Nucleic Acids Res* **28**, 235–242 (2000).

65. Seedorf, H. *et al.* Structure of coenzyme F420H2 oxidase (FprA), a di-iron flavoprotein from methanogenic Archaea catalyzing the reduction of O2 to H2O. *FEBS J* **274**, 1588–1599 (2007).

66. Webb, B. & Sali, A. Comparative Protein Structure Modeling Using MODELLER. *Curr Protoc Bioinformatics* **54**, (2016).

67. Romão, C. V. *et al.* Structure of Escherichia coli Flavodiiron Nitric Oxide Reductase. *J Mol Biol* **428**, 4686–4707 (2016).

68. Schrödinger Release 2023-1. BioLuminate. Preprint at (2021).

69. Schrödinger Release 2023-1. Maestro. Preprint at (2021).

Acknowledgements

We thank Pauli Kallio for kindly providing plasmids for modular cloning and for helpful discussions, Grzegorz Konert for advice on micrograph image analysis, Laura Wey for valuable discussions, and Anniina Lepistö, Janette Vähäsarja, Sofia Westerlund, Ville Käpylä, and Linda Nevala for technical assistance with the experiments. Biophysical experiments were performed within the PHOTOSYN infrastructure at the University of Turku, and confocal microscopy at the Cell Imaging and Cytometry Core, Turku Bioscience Centre, with the support of Biocenter Finland. We also thank the bioinformatics (J.V. Lehtonen), translational activities, and structural biology FINStruct infrastructure support from Biocenter Finland and CSC IT Center for Science for computational infrastructure support at the Structural Bioinformatics Laboratory, (SBL) Åbo Akademi University. Research was funded by Academy of Finland project no. 315119 (to Y.A.), the NordForsk Nordic Center of Excellence 'NordAqua' (no. 82845), and the China Scholarship Council (CSC) Grant no. 201406320187 (to Y.W.).

Contributions

L.N. and Y.A. conceived the idea and designed the experiments. L.N. performed most experiments and analysed the data. S.V. performed the computational modelling. A.S.S. and M.H. contributed

additional cloning, generation of BiFC strains and MIMS. Y.W. and M.B. generated the Fed mutants. K.G. and Y.A. provided resources. Y.A., T.A.S. and K.G. supervised the research. L.N. and Y.A. wrote the article with contributions from all authors.